Supplementary Materials

Electrostatic potential-tuned *d*-band center for enhanced oxygen evolution of NiFe-based catalysts

Chunyang Zhang[a,1], Mingyue Du[a,1], Saiya Liu[a], Wenjia Gu[a], Yitao Si[a,*], Xiaojing Ma[c,*], Maochang Liu[a,b,c*]

[a]*International Research Center for Renewable Energy, State Key Laboratory of Multiphase Flow, Xi'an Jiaotong University, Xi'an, Shaanxi 710049, P. R. China*

[b]*Suzhou Academy of Xi'an Jiaotong University, Suzhou, Jiangsu 215123, P. R. China*

[c]*College of Electrical Engineering, Xinjiang University, Urumqi, Xinjiang 830017, P. R. China*

[1]*Contributed equally to this work.*

**Corresponding author.*

E-mail address: zetuch@stu.xjtu.edu.cn (Y. Si); maxiaojing1983@xju.edu.cn (X. Ma); maochangliu@mail.xjtu.edu.cn (M. Liu)

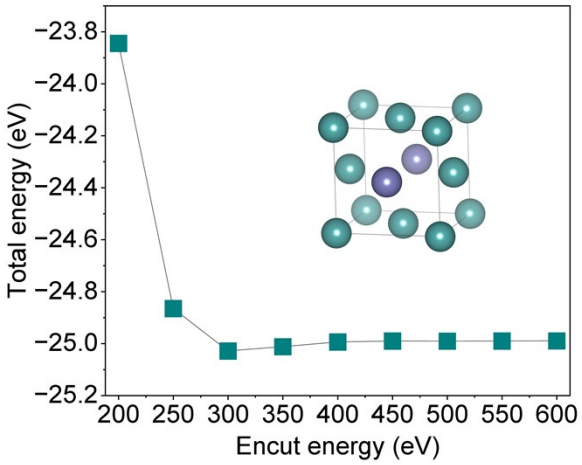

Figure S1. Convergence test of cutoff energy for the Ni_3Fe bulk system.

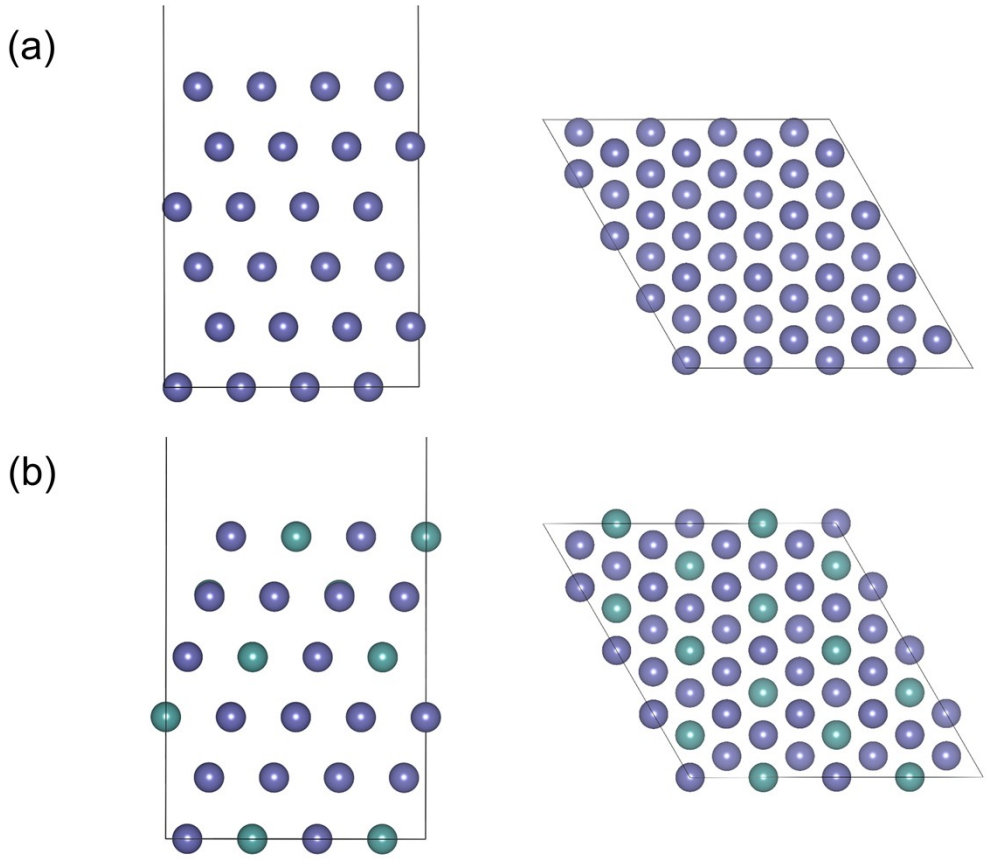

Figure S2. Structural models of Ni_4 and Ni_3Fe. (a) Ni_4. (b) Ni_3Fe. Configurations of Ni_2Fe_2 and $NiFe_3$ are structurally analogous to Ni_3Fe, differing in in their Ni:Fe compositional ratio.

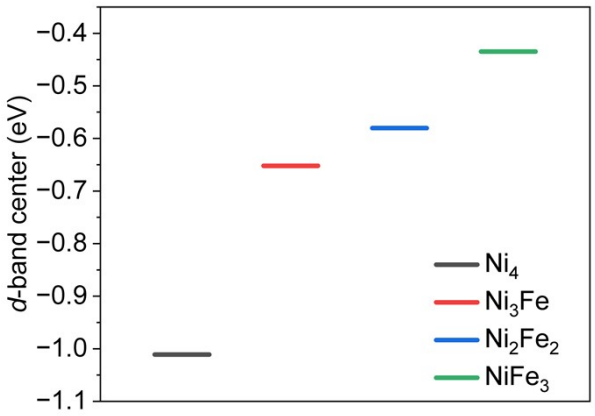

Figure S3. *d*-band centers of NiFe alloys with varying compositions on (111) surfaces.

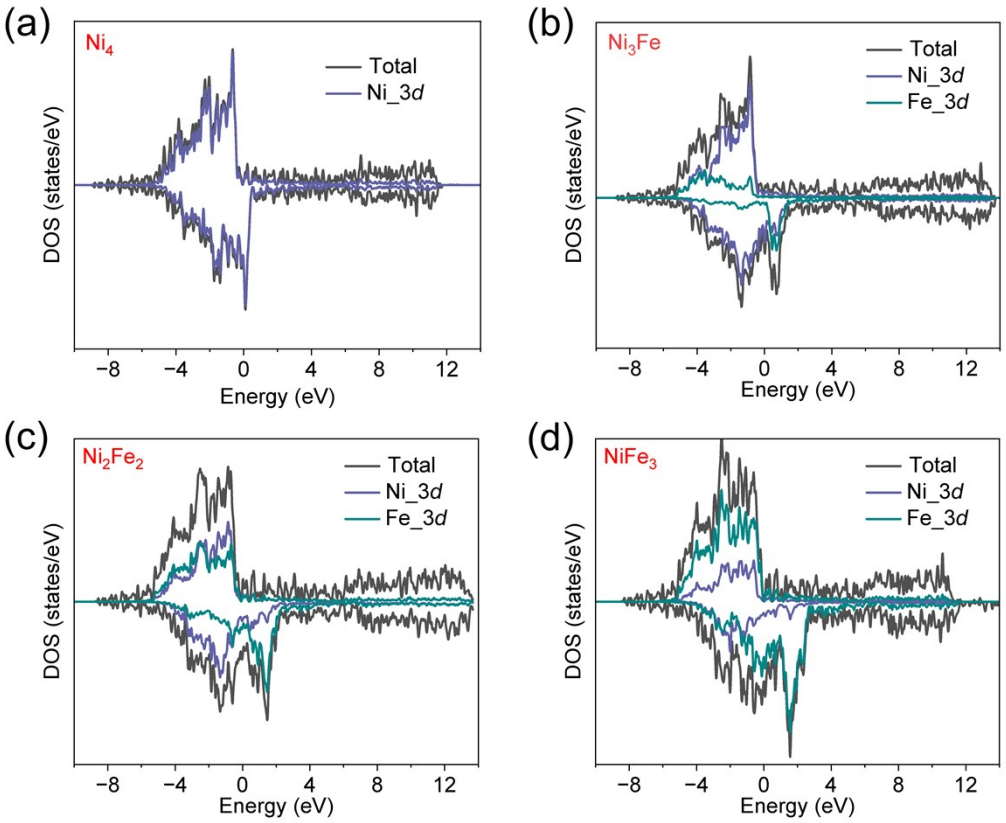

Figure S4. Density of states (DOS) for NiFe alloys with varying compositions on (111) surfaces.
(a) Ni_4. (b) Ni_3Fe. (c) Ni_2Fe_2. (d) $NiFe_3$.

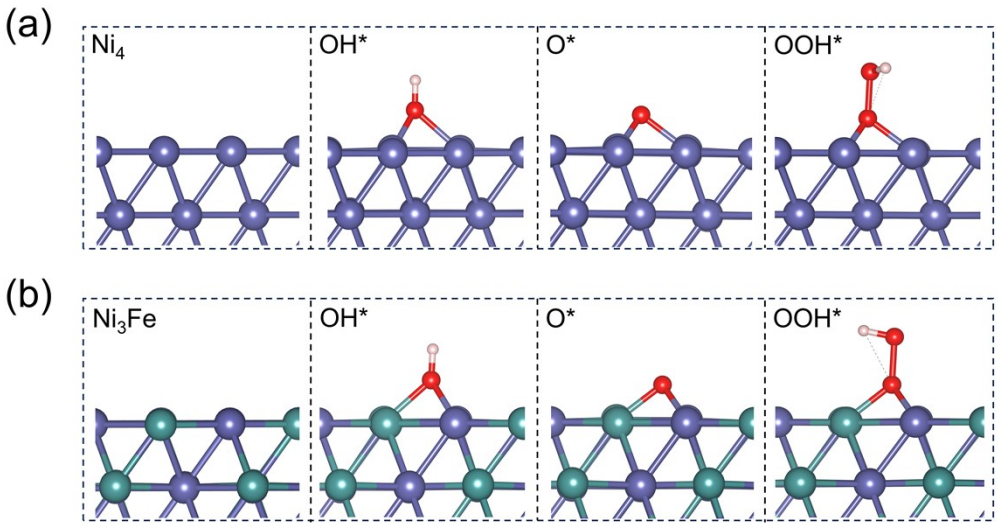

Figure S5. Schematic models of OER processes. (a) Ni_4. (b) Ni_3Fe. Atomic color codes: Purple spheres for Ni, dark cyan spheres for Fe, red spheres for O, white spheres for H.

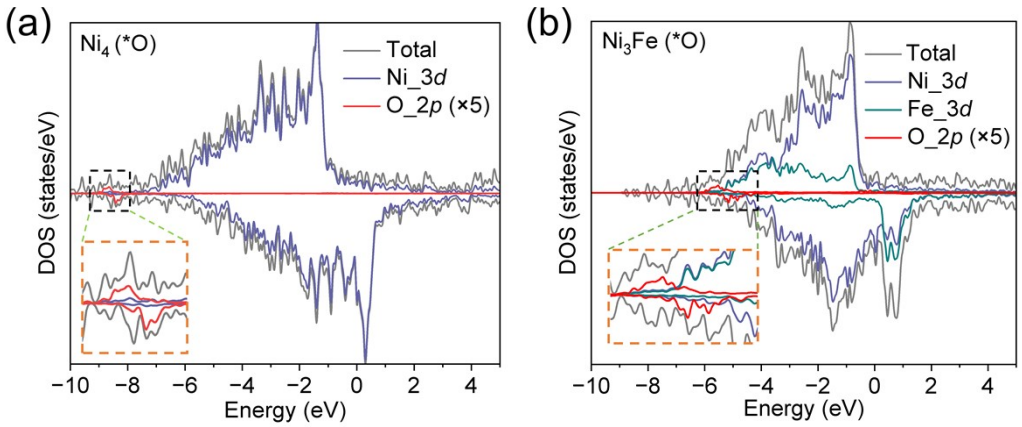

Figure S6. DOS for alloy systems after single oxygen atom adsorption. (a) Ni_4. (b) Ni_3Fe. Insets highlight local DOS features.

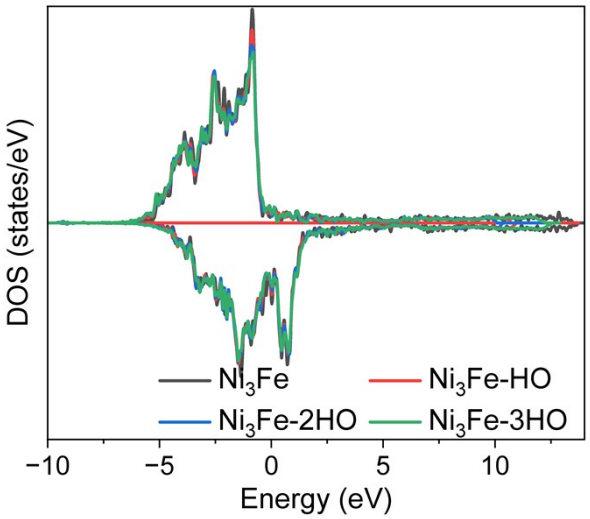

Figure S7. DOS for Ni_3Fe (111) surfaces across varying coverages of O/OH adsorbates.

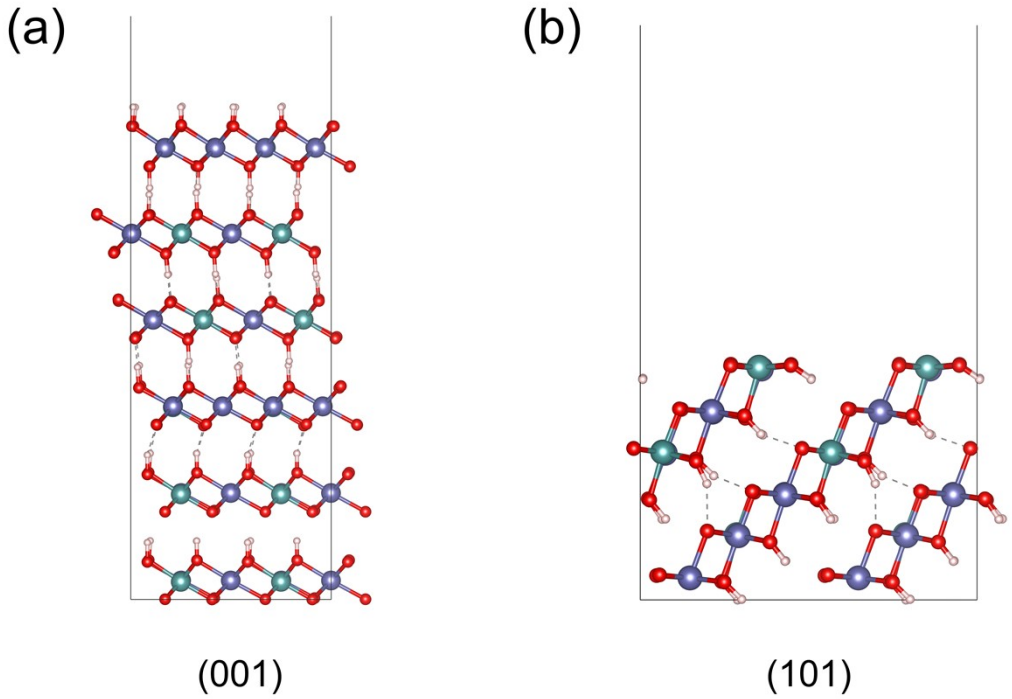

Figure S8. Structural models of NiFeOOH surface. (a) (001) surface. (b) (101) surface. Atomic color scheme: Purple spheres for Ni atoms, dark cyan spheres for Fe atoms, red spheres for O atoms, white spheres for H atoms.

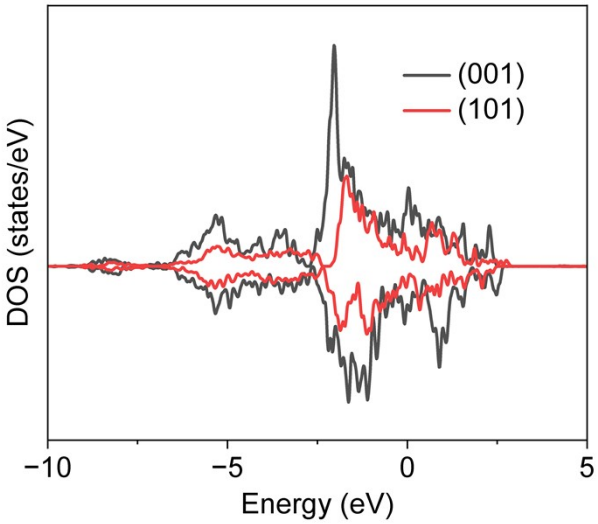

Figure S9. 3*d*-orbital PDOS for NiFeOOH (001) and (101) surfaces.

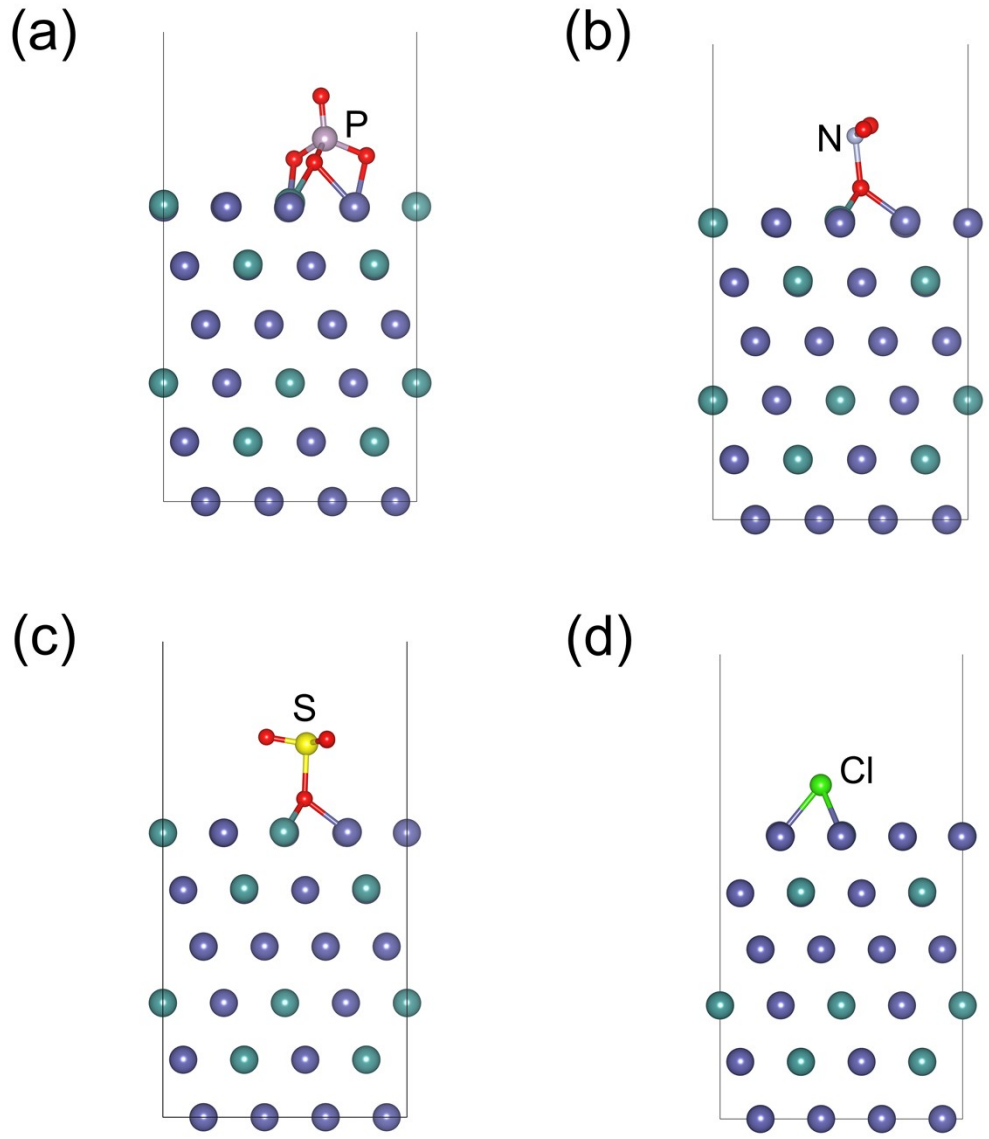

Figure S10. Surface models of $Ni_3Fe(111)$ with adsorbed ions. (a) PO_4^{3-}. (b) NO_3^-.(c) SO_4^{2-}. (d) Cl^-.

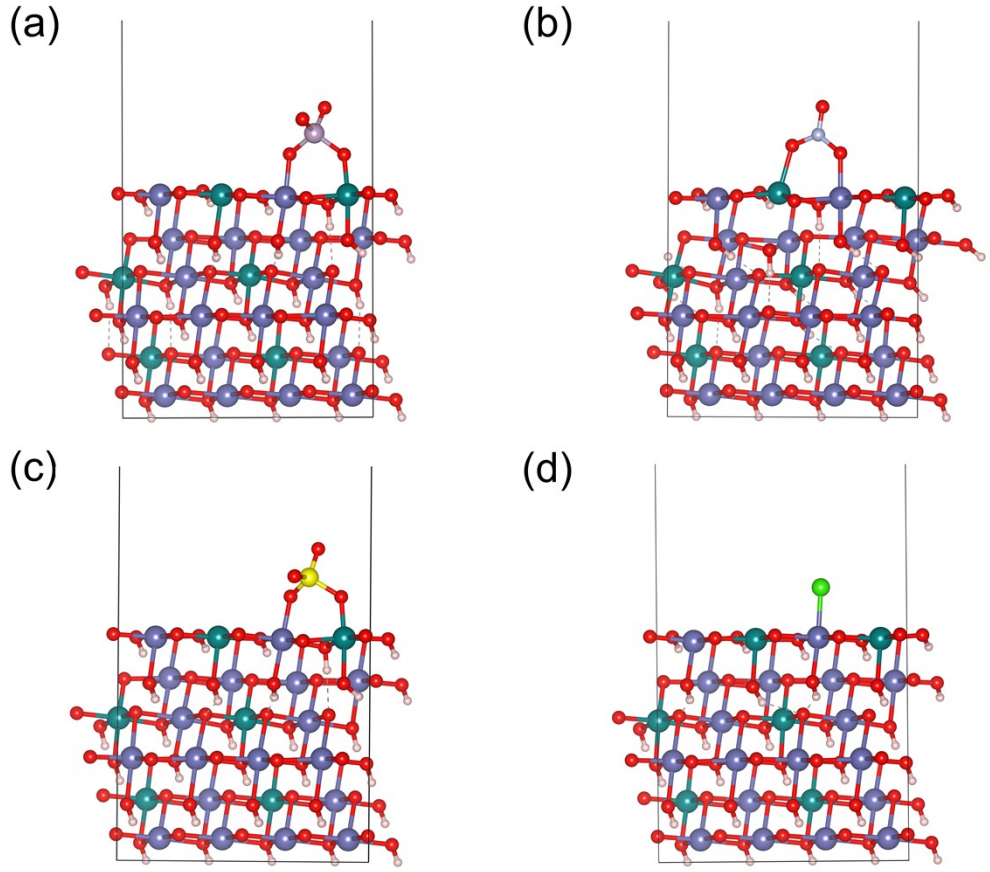

Figure S11. Surface models of NiFeOOH (111) with adsorbed ions. (a) PO_4^{3-}. (b) NO_3^-.(c) SO_4^{2-}. (d) Cl^-.

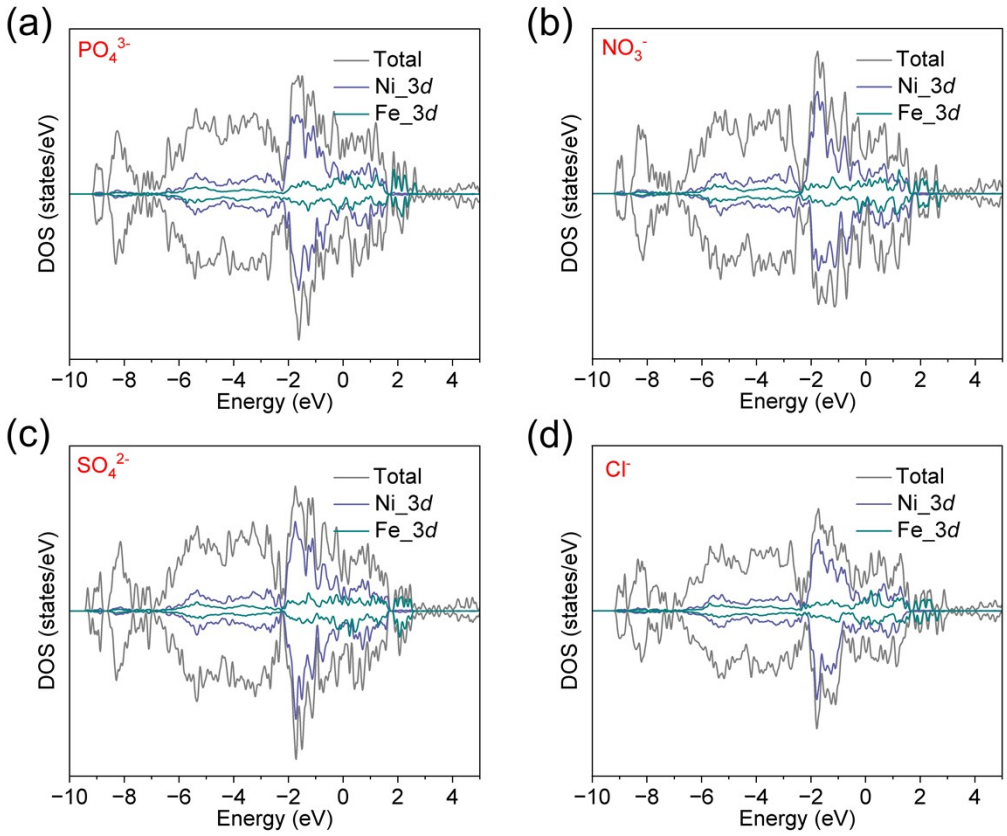

Figure S12. DOS of NiFeOOH (101) surface by adsorbed ionic species. (a) PO_4^{3-}. (b) NO_3^{-}.(c) SO_4^{2-}. (d) Cl^{-}.

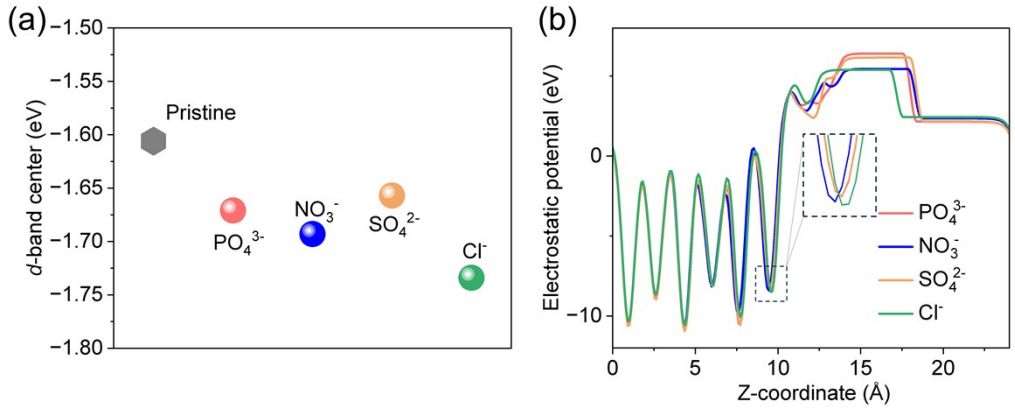

Figure S13. Electronic modifications of NiFeOOH (101) surface by adsorbed ionic species. (a) *d*-band center shifts. (b) ESP maps for different systems.

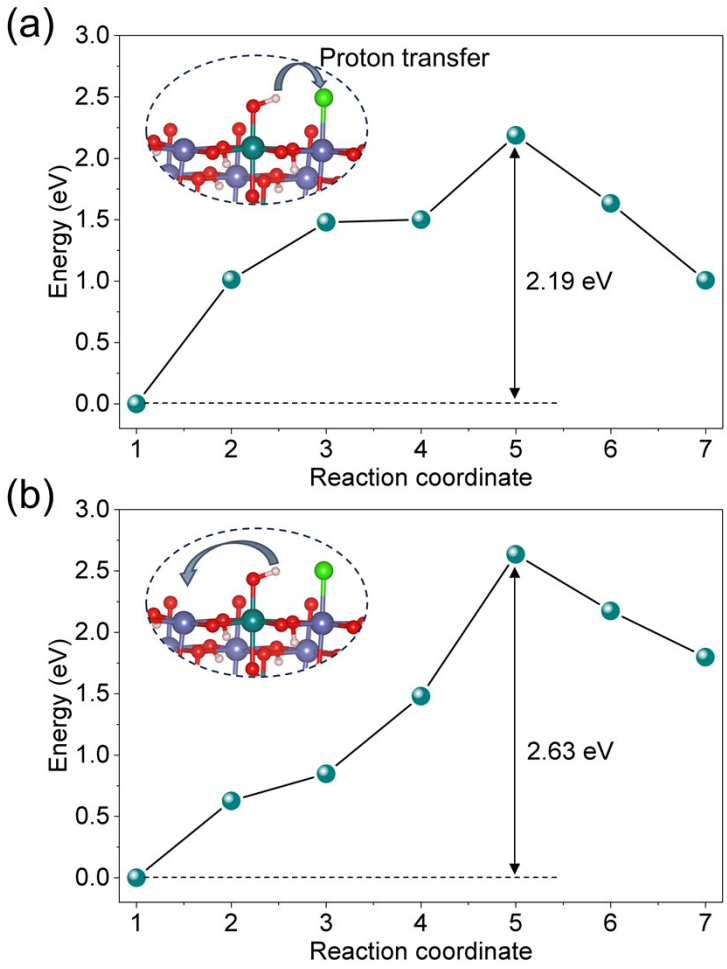

Figure S14. Energy barrier for proton transfer via two different pathways. (a) Transfer from OH* to a Cl atom; (b) Transfer from OH* to an adjacent Ni atom.

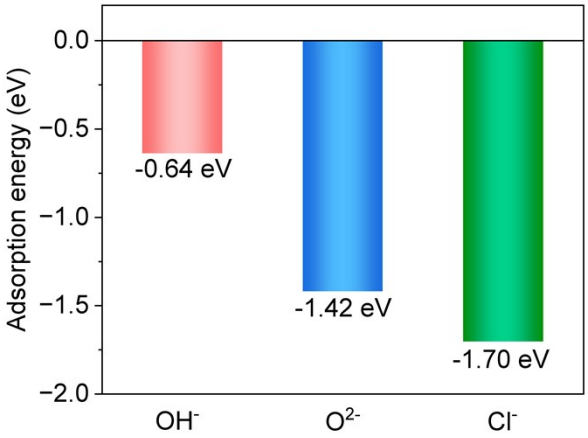

Figure S15. Comparison of adsorption energies of OH^-, O^{2-}, and Cl^-.